Ninth International Conference on CFD in the Minerals and Process Industries
CSIRO, Melbourne, Australia
10-12 December 2012

Experimental and numerical modelling of nasal spray atomisation

Man Chiu Fung[1], Kiao Inthanvong[1], William Yang[2] and Jiyuan Tu[1]

[1] School of Aerospace, Mechanical and Manufacturing Engineering, RMIT University, AUSTRALIA
[2] CSIRO Process Science and Engineering, Clayton, Victoria 3169, AUSTRALIA

ABSTRACT

Spray atomization is a common process found in different industries, where sprays under high injection pressure are widely recorded in the literature. Nonetheless, research on spray breakup mechanism under low pressure in pharmaceutical industry is still relatively rare. Numerical model in the Lagrangian approach was modified for simulating the spray formation from a nasal spray device in the current study. The Linear Instability Sheet Atomization (LISA) was applied to model the formation of spray droplets of a continuous spray from a pressure swirl atomizer. The secondary breakup of spray droplets was simulated by the Taylor Analogy Breakup (TAB) model. Two way momentum coupling was applied to handle the interaction between the gas and liquid phases. The droplet size distribution from numerical solution agreed with experimental result in literature. The external spray characteristics was also studied for comparison. Experimental work of unsteady spray was also performed to study the spray atomization from a nasal spray device. High speed camera and Particle/Droplet Image Analysis (PDIA) were used to determine the spray external characteristics. The atomization stages were defined into pre-stable, stable and post-stable stages, based on the spray cone width. The spray intensity and spray cone dimension were used to evaluate the drug delivery efficiency in different stages. The experimental data is a stepping stone for the validation of a numerical model for unsteady application.

NOMENCLATURE

Symbols

a_1, a_2, a_3	drag coefficient constants applied to smooth spherical droplets over several ranges of droplet Reynolds number
d, D	droplet diameter
d_0	volume median diameter
D_{30}	volume mean diameter
D_{32}	Sauter mean diameter
$\vec{F}$	Additional acceleration term
g	gravitational acceleration
h	liquid sheet thickness
k	turbulent kinetic energy
k_w	atomization wave number, defined as $k_w = \frac{2\pi}{\lambda}$
$\dot{m}$	mass flow rate
M	mass
M_p	momentum exchange between droplets and air
Oh	Ohnesorge number, defined as $Oh = \frac{\sqrt{We}}{Re}$
P	pressure
q	spread parameter
Re	Reynolds number
r	droplet radius
r_0	the radial distance from the axial line to the mid-line of liquid sheet at atomizer exit
t	time
u, U	velocity
V_{slip}	slip velocity
$\vec{v}$	velocity vector of air
We	Weber number defined as $we = \frac{\rho_g v_{slip}^2 r}{\sigma}$

Greek characters

ε	turbulent dissipation
θ	spray half cone angle
σ	liquid surface tension
σ_g	geometric standard deviation
ρ	density
η_0	initial wave amplitude
μ	dynamic viscosity
ω	complex growth rate, defined as $\omega = \omega_r + i\omega_i$

Superscript/subscripts

d	droplet phase
g	gas phase
i, j, k	tensor coordinates
l	liquid
n	*nozzle*

INTRODUCTION

Nasal spray is a relatively new drug delivery method in the pharmaceutical industry. The vascularised mucosa and blood vessels network in nasal cavity has provided a quick delivery route for systemically acting drugs. Other traditional ways, such as oral delivery and intravenous often lead to drug formulation degradation or patient non-compliance related to injection pain. Since nasal spray has advantages over traditional methods, it is worth to investigate the drug delivery mechanism and its applications.

In vivo and in vitro studies of nasal spray are available extensively in literatures. For in vivo study, Suman et al. (2002) applied gamma scientigraphy imaging to study the effect of varying droplet size and spray plume shapes on the deposition pattern. Cheng et al. (2001) has also determined the deposition of spray droplets from nasal spray device in human nasal cavity replica. The spray angle and droplet size were found to be important factors in influencing the deposition pattern. For in vitro testing, Suman et al. (2002) compared the spray properties of two spray bottles by automated actuation system. It was found that the differences in spray pattern, plume geometry and droplet size did not translate to differences in deposition pattern in nose. Dayal et al. (2004) undertook a parametric study to determine the relationship between actuation force, rheological properties of the drug formulation, actuation distance, nasal spray design with droplet size distribution. Guo and Doub (2006) performed a similar study, but they related spray characteristics with actuation velocity and acceleration. Cheng et al. (2001) studied the spray droplet size distribution and cone angle by laser diffraction and still photographic images. A recent research by Inthavong et al. (2012) studied the external characteristics and droplet size of continuous spray from nasal spray device by particle image velocimetry (PIV) and Particle/Droplet Image Analysis (PDIA) and it is the used to validate the numerical model in this study.

Due to the advancement of computational power and numerical modelling techniques, computational fluid dynamics (CFD) was also widely applied for the prediction of spray droplets deposition in nasal cavity (Inthavong et al. 2006; Kimbell et al. 2007). In both of these studies, spray droplet breakup models were not included in simulations. The droplets' size were predefined and being injected at a release point. In order to predict the trajectories and dispersion of spray, the spray cone angle and initial injection velocity were defined.

In current study, the external characteristics and spray droplet size distribution of continuous spray from nasal spray was determined by numerical modelling. The experimental work for unsteady spray was also included herein to provide data for the validation of the current numerical model for unsteady spray in the future.

EXPERIMENTAL SETUP

Spray bottle

A commercially available nasal spray kindly provided by GlaxoSmithKline was used in current study. The volume of the spray bottle has the capacity to provide 200 sprays as shown on the product label. A water tank filled with distilled water was attached to the nasal spray bottle, thus the spray bottle was kept fully filled during the experiment.

Automated Actuation and Image Acquisition

The automated actuation system comprised of a spray bottle holder, a programmable logic control unit (PLC), pneumatic valves and a pneumatic actuator (Figure 1). The spray bottle was fixed on a stand, thus the undesired lateral motion was avoided during actuation. The pressing and releasing motion on nasal spray bottle was executed by a pneumatic actuator. The actuation speed of pressing and releasing was managed by two speed controllers on the pressure line. The PLC unit was used to control the open and close motion of the pneumatic valves, and thus the motion of the actuator. The internal timers and counters of the PLC manipulate the time between actuations and the number of actuations. The strength of actuation force varies with the pressure of compressed air and was controlled by a pressure regulator which limits the pressure levels at 3, 4 and 5 bars. The nasal spray bottle was held in its initial position for 2.5 seconds before extending, and applying a compression force on the spray bottle. The actuator will retract to the initial position immediately after the nasal spray bottle nozzle reached its bottom position. The motion cycle was repeated for 200 cycles for image acquisition. A time of 2.5 seconds between each actuation was determined by Particle and Droplet Image Analysis (PDIA) for sufficient settling of suspended spray droplets from the previous injection.

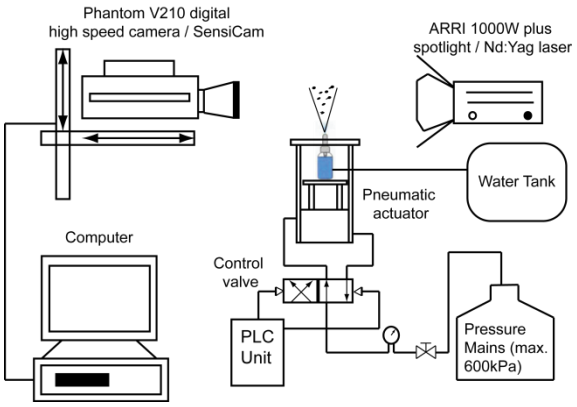

Figure 1: Experimental Setup

For high speed camera filming, a powerful light source was provided by ARRI 1000W plus a manual spotlight to retain short exposure time to capture bright images. Spray images were captured by Phantom V210 digital high-speed camera. The frame rate and exposure time were 2200 per second and 6μs respectively. The motion of the spray bottle nozzle (pressing, holding and releasing) and the development of spray plume were captured for qualitative and quantitative analysis. Three sets of images were recorded under different back pressure (3, 4, 5 bar) to minimize the variance in analysis.

For PDIA, a long distance microscope lens with magnification of 2.46 was attached to SensiCam 128 bit cooled imaging camera. The light source was replaced by Nd: Yag laser. Field of View (FOV) of 3.85 mm× 3.08 mm with resolution of 3.01 μm/pixel was obtained at close to nozzle region at 11 different locations to cover the first 12 mm downstream of spray plume. 100 image pairs were obtained in each FOV for analysis.

NUMERICAL MODEL

The governing equations for the fluid phase are:

$$\frac{\partial}{\partial x_j}\left(\rho_g u_j^g\right) = 0 \quad (1)$$

$$\rho_g \frac{\partial u_i^g}{\partial t} + \rho_g u_j^g \frac{\partial u_i^g}{\partial x_j} = -\frac{\partial p_g}{\partial x_i} + \frac{\partial}{\partial x_j}\left[\mu_g \frac{\partial u_i^g}{\partial x_j}\right] + \frac{1}{\rho_g} M_p \quad (2)$$

The Realizable *k*-*ε* turbulence model is used in current study and its turbulence transport equations are given as:

$$\frac{\partial}{\partial t}(\rho k) + \frac{\partial}{\partial x_i}(\rho k u_j) = \frac{\partial}{\partial x_i}\left[\left(\mu + \frac{\mu_t}{\sigma_k}\right)\frac{\partial k}{\partial x_j}\right] + P_k + P_b - \rho\varepsilon + S_k \quad (3)$$

$$\frac{\partial}{\partial t}(\rho \varepsilon) + \frac{\partial}{\partial x_i}(\rho \varepsilon u_j) = \frac{\partial}{\partial x_i}\left[\left(\mu + \frac{\mu_t}{\sigma_\varepsilon}\right)\frac{\partial \varepsilon}{\partial x_j}\right] + \rho C_1 S_\varepsilon - \rho C_2 \frac{\varepsilon^2}{k+\sqrt{v\varepsilon}} + C_{1\varepsilon}\frac{\varepsilon}{k}C_{3\varepsilon}P_b + S_\varepsilon \quad (4)$$

Primary breakup model

The primary breakup was simulated by the Linear Instability Sheet Atomization (LISA) model. The model assumes that a two-dimensional, viscous, incompressible liquid sheet of thickness $2h$ moving with a relative velocity U through an inviscid, incompressible gas medium. A spectrum of infinitesimal disturbance of the form

$$\eta = \eta_0 e^{ik_w x + \omega t} \quad (5)$$

is imposed on the initially steady motion. The total velocity U is obtained by the relation with injection pressure

$$U = k_v \sqrt{\frac{2\Delta P}{\rho_l}} \quad (6)$$

where k_v is the velocity coefficient calculated by

$$k_v = max\left[0.7, \frac{4\dot{m}}{\pi d_0^2 \rho_l cos\theta}\sqrt{\frac{\rho_l}{2\Delta P}}\right] \quad (7)$$

The thickness of the initial film is determined by the correlation between mass flow rate ($\dot{m}$) nozzle exit diameter d_n, liquid density ρ_l and axial velocity of liquid film, $U\cos\theta$.

$$\dot{m} = \pi \rho_l U \cos\theta\, h(d_n - h) \quad (8)$$

The breakup length L is given by

$$L = \frac{U}{\Omega} ln\left(\frac{\eta_b}{\eta_0}\right) \quad (9)$$

A volume median diameter is produced and is given by

$$d_0 = 1.88 d_l (1 + 3\mathrm{Oh})^{1/6} \quad (10)$$

where d_l is the diameter of ligament formed at the point of breakup

The resultant droplet diameter is incorporated with a Rosin-Rammler distribution function (R-R) to provide the droplet size distribution as

$$f(d) = \frac{q d^{q-1}}{D^q} exp\left\{-\left[\frac{d}{D}\right]^q\right\} \quad (11)$$

Where

$$D^q = \frac{{d_0}^q}{\ln(2)} \quad (12)$$

Additional details of the model is available in Senecal et al. (1999).

Secondary breakup model

The model used herein is the Taylor Analogy Breakup (TAB) model, which is responsible to the breakup of parent droplets formed by LISA model. There are five distinct breakup regime determined by the Weber number of parent droplets. The details are available in Pilch and Erdman (1987).The model equations of TAB model can also be found in ANSYS software manual. (Ansys 2009)

Droplet Modelling

The spray droplets (disperse phase) are simulated in Lagrangian approach. Two-way coupling is applied in the model, so there is momentum exchange between disperse phase and fluid phase. The force balance equations is:

$$\frac{du_p}{dt} = F_D(u_g - u_p) + \frac{\vec{g}(\rho_p - \rho_g)}{\rho_p} + \vec{F} \quad (13)$$

F_D is the drag force defined as

$$F_D = \frac{18\mu}{\rho_p {d_p}^2}\frac{C_D Re}{24} \quad (14)$$

The drag coefficient, based on Morsi and Alexander (1972) is given as

$$C_D = a_1 + \frac{a_2}{Re} + \frac{a_3}{Re^2} \quad (15)$$

NUMERICAL SETUP

The computational domain was cylindrical in shape with 1m diameter and 1m height. The geometry was meshed with 2.16 million quad and hexa elements with an O-grid in the centre to get a fine mesh around the spray region, after grid independence test, which is based on spray penetration. (Figure 2)

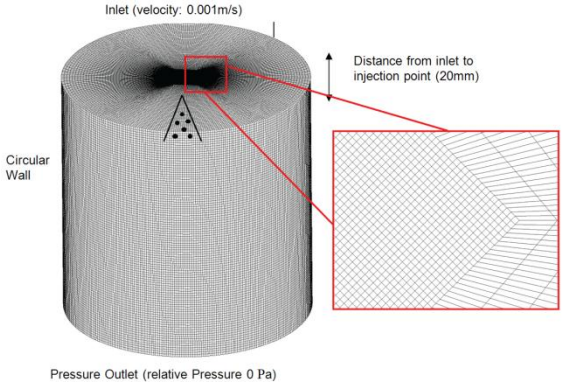

Figure 2: Geometry mesh and boundary conditions.

The CFD code, ANSYS Fluent v12.1 was used to calculate the continuity and the momentum equations for both gas phase and liquid phase. Third order accurate QUICK scheme was applied for the discretisation of these equations, while a second order upwind scheme was used for the turbulent kinetic energy and dissipation rate. The pressure-velocity coupling was solved by SIMPLE scheme and a Runge-Kutta scheme was used for the integration of droplet trajectories. The properties of the liquid and gas phase and injection conditions are based on the study case by Inthavong et al. (2012)

Table 1: properties of liquid and gas phase and injection conditions are based on the research by Inthavong et al.(2012)

Properties of spray	
Density	998.2 kg/m^3
Viscosity	0.001003 kg/m.s
Surface Tension	0.072 N/m
Injection pressure	5 bar
Mass Flow Rate	0.00145 kg/s
Spray Cone Angle	25^o
Nozzle diameter	0.5 mm
Liquid sheet constant	1

Spread parameter Dispersion Angle	2.2 3°
Properties of Air	
Density (kgm^{-3}) Viscosity (kg/m-s) Temperature	1.225 kg/m^3 1.789e-5 kg/m.s 298.15 K

RESULTS

Spray model validation

The spread parameter, q in R-R distribution function (**Eqn.** (11)) is related to the uniformity of size distribution. Smaller value implies a more widely spread distribution. By comparing with experimental droplet size data across eight local regions closed to injection point from Inthavong et al. (2012), it shows that the model provided the best fit when q=2.2 (Figure 3).

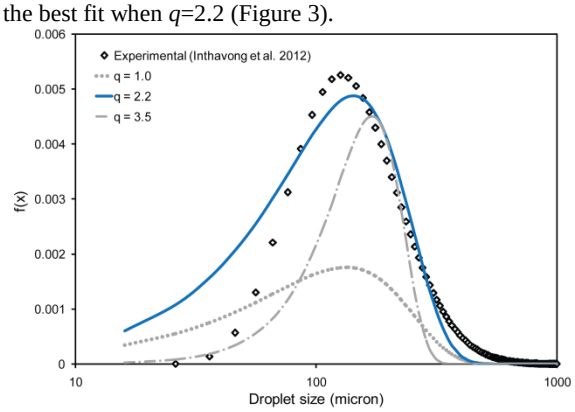

Figure 3: Comparison of volume log-normal distribution of spray droplets from experimental result and the corresponding Rosin Rammler distribution with spread parameter: 2.2.

The liquid sheet constant, $ln\left(\frac{\eta_b}{\eta_o}\right)$ in the LISA model controls the breakup length of liquid sheet, which also influences the liquid sheet thickness and ligament size. For high pressure applications, this value is commonly set to 12. (Gao et al. 2005; Park et al. 2009; Schmidt et al. 1999). By varying the liquid sheet constant and comparing Sauter Mean Diameter (S.M.D.) with experimental data, it was found that the sheet constant 1 provides a good approximation. The original value, 12, gives an exceptionally small droplet size (0.5 µm), which is inaccurate, therefore it is not applicable in low pressure applications (Figure 4). The measurement location and external characteristics of numerical result are illustrated in Figure 5.

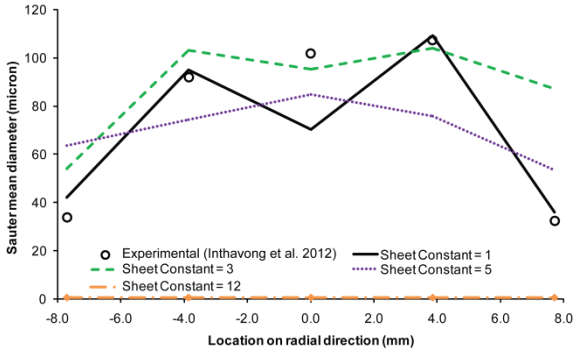

Figure 4: Sauter mean diameter (SMD) of droplets at differnt radial location with various liquid sheet constant at downstream distance between y = 9.246 mm and y = 12.33 mm.

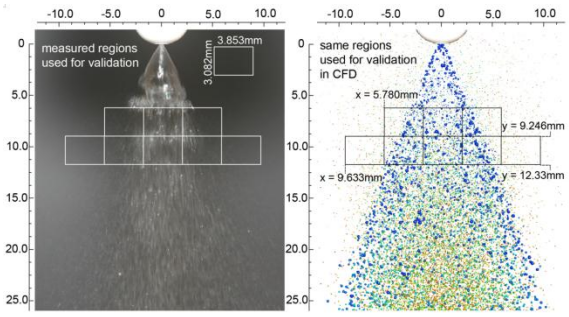

Figure 5: The measurement location and external characteristics of numerical result.

The Mean Volume Diameter (D_{30}) and Sauter mean diameter (D_{32}) were also used for validation. The general form of the system is shown as follow:

$$(\boldsymbol{D_{ab}})^{a-b} = \frac{\int_{D_0}^{D_m} \boldsymbol{D}^a(\frac{dN}{dD})d\boldsymbol{D}}{\int_{D_0}^{D_m} \boldsymbol{D}^b(\frac{dN}{dD})d\boldsymbol{D}} \quad (16)$$

where N is the number of drops, D_0 is the minimum droplet diameter and D_m is the maximum droplet diameter.

The Mean Volume Diameter is the ratio of volume of a sphere to the spheres' number. A larger Mean Volume Diameter indicates a higher dose of delivered liquid with a specific spray droplet number. Sauter Mean Diameter is defined as a sphere with the same volume to surface area ratio. A smaller value represents a higher surface area to volume ratio which implies that the spray droplets provide a larger contact surface area with constant amount of liquid. Lefebvre (1989) stated that this parameter is used for evaluating the performance of mass transfer and reaction, when surface area is the determining factor. Hence, it is useful to evaluate the absorption efficiency of nasal spray in nasal cavity. The comparison of the numerical result with experimental data is shown in

Figure **6**. It was found that the simulation can accurately predict the amount of water delivered at different locations close to nozzle exit. The comparison of Sauter Mean Diameter also has a good agreement. Generally, large droplets are located at the central area along the axial axis of nozzle exit, while small droplets are driven to peripheral regions by turbulence induced flow from the spray itself.

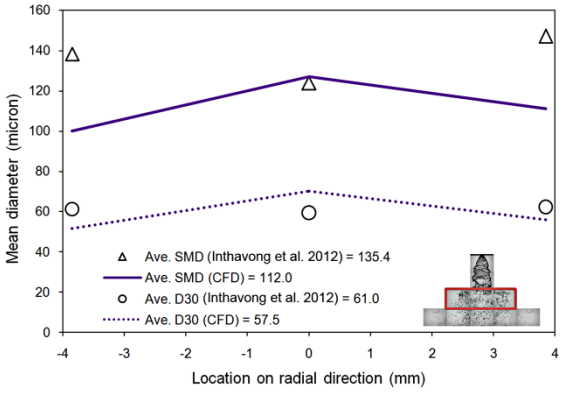

(a)

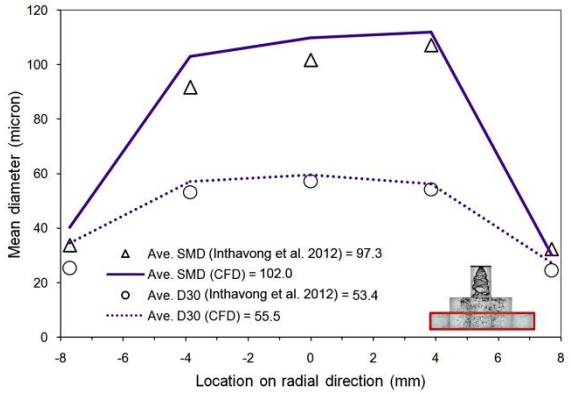

(b)

Figure 6: Comparison of SMD and D_{30} with experimental data from Inthavong et al. (2012)for downstream locations between (a) y = 6.164 mm and y = 9.246 mm (b) y = 9.246 mm and y = 12.33 mm from orifice.

Experimental result

The continuous spray measurement is used for the validation of numerical models. It is not practical in real life, since the operation of a nasal spray device is a pulsing motion. The mass flow rate of liquid passing through atomizer varies during the atomization process. Hence it is worth investigating the external characteristics of the spray to provide data for validating current numerical models.

By the application of a high speed camera, the spray propagation was recorded. For low pressure spray, the spray development can be classified into 4 stages: distorted pencil, onion stage, tulip stage and fully developed spray (Figure 7).

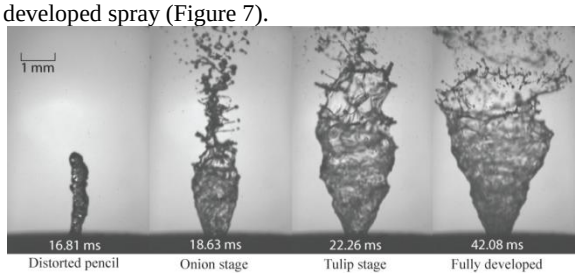

Figure 7: Spray development stages of nasal spray device under 5 bar compression pressure: distorted pencil, onion stage, tulip stage and fully developed.

Formation of pre-spray

At the initial stage of spray, the injection pressure is underdeveloped. The insufficient pressure causes the formation of a pre-spray. The interaction between liquid and gas phase causes aerodynamic instability which leads to early disintegration of the spray ligament and formation of large water blobs. The size of these blobs range between 0.93 mm and 1.13 mm for 3 and 5 bar compression pressure respectively (Figure 8).

According to the nasal cavity geometry studied by Wen et al. (2008), the cross-sectional area of the nasal valve is about 0.7 cm^2 where it is located at 20 mm from the anterior tip of the nose for a 25 years old, healthy Asian male. The width of the nasal valve can be as narrow as 7.8 mm. This means that the exceptionally large size of droplets prevents them from entering the nasal cavity. Thus, the spray droplets from the initial period of atomization have low drug delivery efficiency.

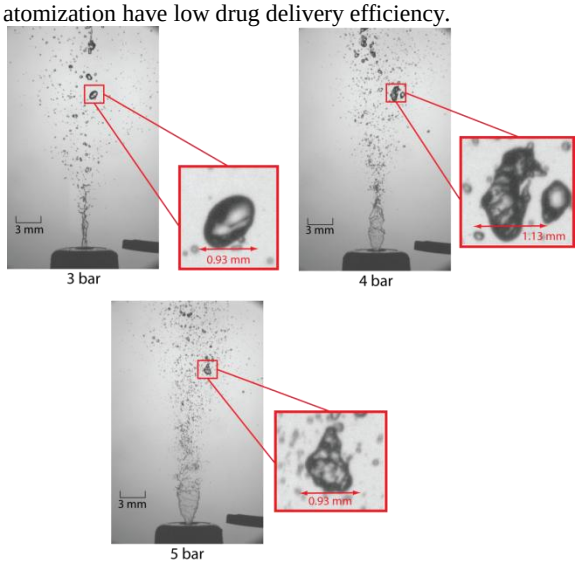

Figure 8: The maximum width of the last water blob formed by pre-spray under different compression pressure varies between 0.93 mm and 1.13 mm

Definition of Spray Stages

In the pharmaceutical industry, the spraying stages are defined by the spray droplet size. The "Stable stage" is defined as the period when spray droplet size is constant and at smallest in the size range. Since the size measurement is not included in this paper, determination of the stable stage is defined by the spray cone width. According to the numerical simulation by Snyder et al (2004), the spray droplet size is inversely proportional to the spray cone angle. In the other words, spray cone width is a valid criteria for defining spray stages. The "Stable stage" can be defined as the period with widest spray cone width. The stages before and after this are termed "Pre-stable stage" and "Post stable stage" respectively.

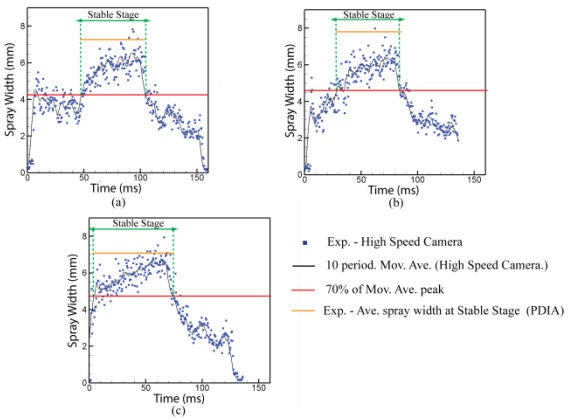

Figure 9: The variation of spray width at 4.4 mm downstream from injection point under different injection pressure. (a) 3 bar (b) 4 bar (c) 5 bar. The stable stage is defined at 70% of the moving average peak.

The spray cone width was determined by the utilisation of image processing tool in MATLAB at 9.22 mm downstream from the injection point. The photos were converted to binary image based on greyscale threshold criteria for analysis. By scanning each pixel per row and column of each image, the total number of columns with

white pixels (filled with water) can be converted to the spray cone width. The value at 70% of the peak of the moving average value for the spray width is defined herein as a threshold for the stable stage of spray. The result was further validated with PDIA data for consistency and repeatability (Figure 9).

Spray Intensity

The spray intensity value in the field of view of 26.1 mm (axial)× 17.8 mm (radial width) at the middle of the spray stages under various compression pressure was obtained by MATLAB and normalized at fixed timing during the middle of each spray stage (Figure 10). The highest intensity value is one, which defined as the axial location with largest amount of liquid located. It normally occurs in the axial axis of nozzle exit. As stated before, the nasal valve is limited in size and constraints the delivery of spray to the nasal cavity, only the spray located in the "effective region" has highest probability to enter nasal cavity. It shows that the highest delivery efficiency always occur at the stable stage of the atomization.

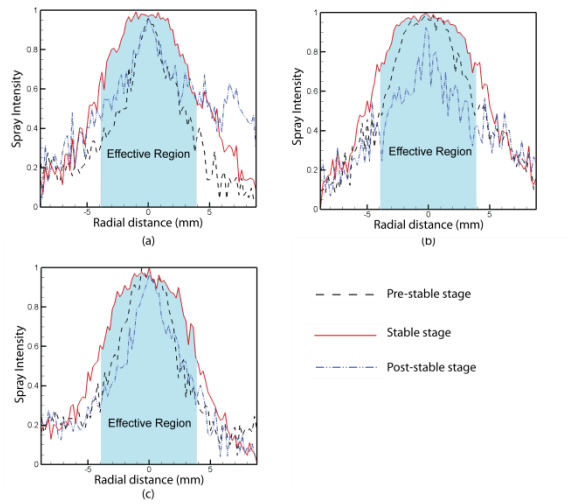

Figure 10: Spray Intensity (a)3 bar (b)4 bar (c) 5 bar

CONCLUSION

The study demonstrated the validity of the current numerical spray breakup model for a continuous spray from the nasal spray device. By adjusting the liquid sheet constant and spread parameter of the Rosin-Rammler distribution, the model gives a prediction of the spray plume shape and droplet size distribution (D_{30}, D_{32}) for low pressure application. The experimental phase of the study of unsteady spray from nasal spray device was also performed herein. By using of high speed camera and particle droplet image analysis technique, the external characteristics of the transient development of a spray cone were captured for analysis. The definition of spray stages is defined and the spray intensity analysis was discussed. This study is a stepping stone to provide data for validation of the numerical model in future.

REFERENCES

ANSYS (2009). *CFX 12.1 Solver Theory*. Ansys Inc., Canonsburg, PA.

CHENG, Y. S., HOLMES, T. D., GAO, J., GUILMETTE, R. A., LI, S., SURAKITBANHARN, Y. and ROWLINGS, C. (2001). Characterization of nasal spray pumps and deposition pattern in a replica of the human nasal airway. *J. Aerosol Med.* 14:267-280.

DAYAL, P., SHAIK, M. S. and SINGH, M. (2004). Evaluation of different parameters that affect droplet-size distribution from nasal sprays using Malvern Spraytec. *J. Phar. Sci.* 93:1725-1742.

GAO, J., JIANG, D., HUANG, Z. and WANG, X. (2005). Experimental and numerical study of high-pressure-swirl injector sprays in a direct injection gasoline engine. *Proceedings of the I MECH E Part A Journal of Power and Energy* 219:617.

GUO, C. and DOUB, W. H. (2006). The influence of actuation parameters on in vitro testing of nasal spray products. *J. Pharm. Sci.* 95:2029-2040.

INTHAVONG, K., TIAN, Z. F., LI, H. F., TU, J. Y., YANG, W., XUE, C. L. and LI, C. G. (2006). A numerical study of spray particle deposition in a human nasal cavity. *Aerosol Sci. Technol.* 40:1034-1045.

INTHAVONG, K., YANG, W., FUNG, M. C. and TU, J. Y. (2012). External and Near-Nozzle Spray Characteristics of a Continuous Spray Atomized from a Nasal Spray Device. *Aerosol Sci. Technol.* 46:165-177.

KIMBELL, J. S., SEGAL, R. A., ASGHARIAN, B., WONG, B. A., SCHROETER, J. D., SOUTHALL, J. P., DICKENS, C. J., BRACE, G. and MILLER, F. J. (2007). Characterization of deposition from nasal spray devices using a computational fluid dynamics model of the human nasal passages. *J. Aerosol Med.* 20:59-74.

LEFEBVRE, A. H. (1989). *Atomization and sprays*. Hemisphere Pub. Corp., New York.

MORSI, S. A. and ALEXANDER, A. J. (1972). An investigation of particle trajectories in two-phase flow systems. *J. Fluid Mech.* 55:193-208.

PARK, S. H., KIM, H. J., SUH, H. K. and LEE, C. S. (2009). Atomization and spray characteristics of bioethanol and bioethanol blended gasoline fuel injected through a direct injection gasoline injector. *Int. J. Heat Fluid Fl.* 30:1183-1192.

PILCH, M. and ERDMAN, C. A. (1987). Use of breakup time data and velocity history data to predict the maximum size of stable fragments for acceleration-induced breakup of a liquid drop. *Int. J. Multiphas. Flow* 13:741-757.

SCHMIDT, D. P., NOUR, I., SENECAL, P. K., RUTLAND, C. J., MARTIN, J. K. and REITZ, R. D. (1999). Pressure-Swirl Atomization in the Near Field. *SAE Technical Paper* 1999-01-0496.

SENECAL, P. K., SCHMIDT, D. P., NOUAR, I., RUTLAND, C. J., REITZ, R. D. and CORRADINI, M. L. (1999). Modeling high-speed viscous liquid sheet atomization. *Int. J. Multiphas. Flow* 25:1073-1097.

SNYDER, J. A., GROVER, R. O., JR., V. S. and ASSANIS, D. N. (2004). Transient Spray Cone Angles in Pressure-Swirl Injector Sprays. *SAE Techical Paper* 2004-01-2939.

SUMAN, J. D., LAUBE, B. L., LIN, T. C., BROUET, G. and DALBY, R. (2002). Validity of in vitro tests on aqueous spray pumps as surrogates for nasal deposition. *Pharma. Res.* 19:1-6.

WEN, J., INTHAVONG, K., TU, J. Y. and WANG, S. (2008). Numerical simulations for detailed airflow dynamics in a human nasal cavity. *Resp. Physiol. Neurobi.* 161:125-135.